Complementary Approach for Reliable High Speed Transmission Line Protection

Elmo Price, ABB Inc.

Torbjorn Einarsson, ABB AB

***Abstract*— Line distance protection technology has evolved from sound operating principles using phase comparators used in electromechanical relays to the present day relays using microprocessor technology. Initial microprocessor relays used full cycle Discrete Fourier Transformation to extract the fundamental phasors from sampled analog data and apply them in comparator equations to determine impedance reach. This technique is still being used in most the modern microprocessor relays today. In order to address the effects of dc offset and CCVT transients a compromise is however required between operating speed, reach and security. Also, their performance is relatively independent of Source Impedance Ratio (SIR) once the transients have subsided, usually in two to three cycles. A totally different approach was introduced in 1997 using a time domain algorithm that mimics the operation of the electromechanical phase comparator. This algorithm proved to be one of the fastest and most secure for protection of medium and long lines typical for distance protection applications. The only compromise with this algorithm is the higher operating time for very short lines with high Source Impedance Ratios. This paper discusses the relative performances of each of the above approaches individually and about the advantages of combining the two algorithms to run in parallel.**

***Index Terms*—Protective relaying, distance measurement, phase comparators**

I. Nomenclature

TD – time domain algorithm
DFT – Discrete Fourier Transform algorithm
CCVT – Coupling Capacitor Voltage Transformer
SIR – Source Impedance Ratio

II. Introduction

Reliable high speed line distance protection is desirable to ensure system stability of the modern power system and to minimize fault damage. Some utility applications require sub-cycle line fault detection to initiate fault clearing, We are, however, always faced with the reliability equation requiring dependable tripping for all line faults as fast as possible, but at the same time being secure against tripping for external line faults. Algorithms have been employed that offer security and dependability at the cost of speed, or speed at the cost of dependability or security. In the end there are two principles that are trying to be addressed by one protection algorithm – speed and reliability (security and dependability). Often redundant line protection terminals are provided to optimize the two desired characteristics. This paper discusses the feasibility of using two distinctly different phase comparator methods, which have been employed in real system applications for more that ten years, to complement each other.

We will begin the discussion with a review of the phase comparator principle used in line distance protection employing mho impedance characteristics, and the effect of CCVT subsidence transients on distance measurement. Two different, but field-proven, numerical methods will be discussed reviewing their application and performance and the advantages and disadvantages of each. This will then be followed by a discussion as to how they are used to complement each other to overcome shortcomings in each and provide reliable high-speed performance.

III. Phase Comparator

A. Basic Phase Comparator Principle

Transmission line distance relays have long employed phase and magnitude comparators to accurately determine faults internal or external to a defined region. A magnitude comparator is a design element used to compare magnitudes of two phasors and a phase comparator compares their phase angle relationship. Much has been written on the subject of magnitude and phase comparators [2][4], therefore, this discussions focuses only on the phase comparator. Fig. 1 shows the basic phase comparator principle. The comparator processes the two input phasors, S_1 and S_2, determines the phase angle relationship between them and then outputs the results, operated or not operated. Phase comparators are used in a broad range of applications that define fault direction and impedance characteristics.

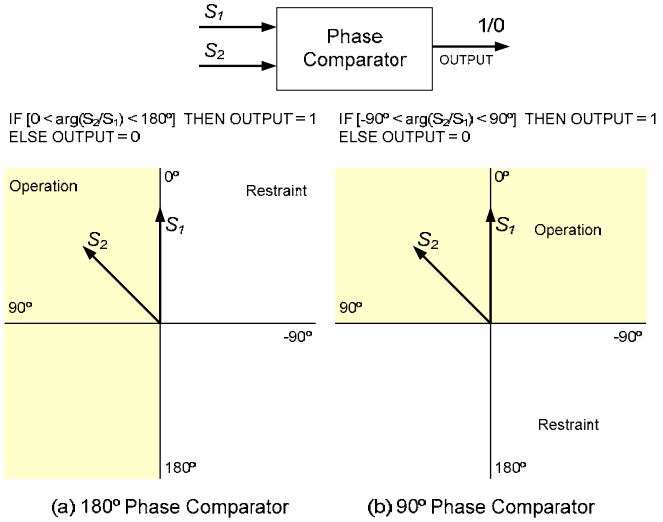

Fig. 1. Typical Phase Comparators

B. Phase Comparator for Mho Characteristics

The phase comparator inputs for defining mho distance characteristics are voltage phasors, which are defined by the impedance loops they are measuring, AG, BG, CG, AB, BC, CA or ABC.

To understand phase comparator for the mho characteristic it is easier to look at the relationship of impedances in the voltage (IZ) plane where the mho characteristic is defined by the voltage drops across the respective impedances. First, we will consider the operation of the self polarized characteristic.

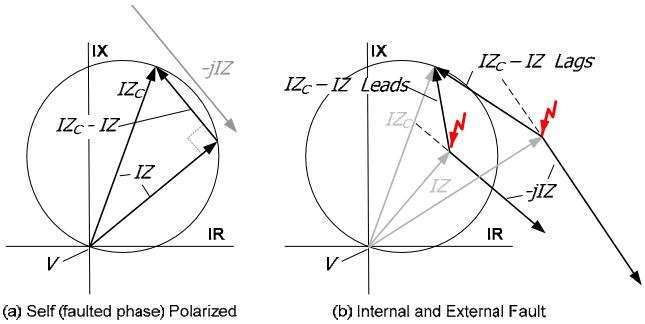

Fig. 2. Self Polarized Mho Characteristics

Figure 2 shows a non-compensated single phase mho characteristic that is self polarized. The same analysis will apply when considering phase-to-phase and ground fault loops with the appropriate fault voltages, currents and impedances. The relay compensator reach setting is Z_C and the apparent fault impedance as measured at the relay is Z. The fault voltage measured at the relay is V and the fault current is I. We can develop an operating voltage V_{OP} that subtracts the measured voltage drop from the relay to the fault, V, from the compensator voltage, IZ_C. For a fault on phase A the self polarizing voltage is fault voltage V_A and the fault current is I_A. This provides the following simple equations:

$$V_{OP} = I_A Z_C - V_A = I_A Z_C - I_A Z \quad (1)$$

$$V_A = I_A Z \quad (2)$$

From Figure 2(a), where $I = I_A$ and $V = V_A$, we can see that the locus of points for all fault impedance angles where the vectors IZ and IZ - IZ_C are perpendicular will define a circle of diameter IZ_C. Therefore, the comparison of angle between IZ and IZ- IZ_C, likewise V_A and V_{OP}, will determine if the fault is an internal or external. To achieve correct operation using the phase comparator of Figure 1(a) with the above voltages we have:

$$S_1 = -jV_A = -jI_A Z \quad (3)$$

$$S_2 = I_A Z_C - V_A = I_A Z_C - I_A Z \quad (4)$$

Analyzing the comparison of S_1 *(-jIZ)* and S_2 *(IZ_C - IZ)* we can see that for fault impedance voltages *IZ* on the boundary of the circle and lagging IZ_C, S_1 and S_2 are 180º apart. For a fault impedance voltage *IZ* inside the circle characteristic and lagging IZ_C, S_2 will lead S_1 from 90º to 180º. For the fault impedance voltage IZ that is in phase with IZ_C, S_2 leads S_1 by 90º. Where the fault impedance voltage IZ leads IZ_C and is within the characteristic, S_2 will lead S_1 from 90º at the center line (on IZ_C) to 0º at the boundary (the circle). Where the fault impedance voltage IZ is external to the characteristic, S_2 will lag S_1.

Now consider the cross or healthy phase mho characteristic as shown in Figure 3. The analysis is the same; however, we will be comparing the angular relationship of $-jIZ_F$ and IZ_C - *IZ*. In this case IZ_F is the sum of the source impedance voltage drop IZ_S and the fault impedance voltage IZ as measured by the relay. The source voltage on phase A is defined by:

$$V_{SA} = I_A(Z_S + Z) = I_A Z_F \quad (5)$$

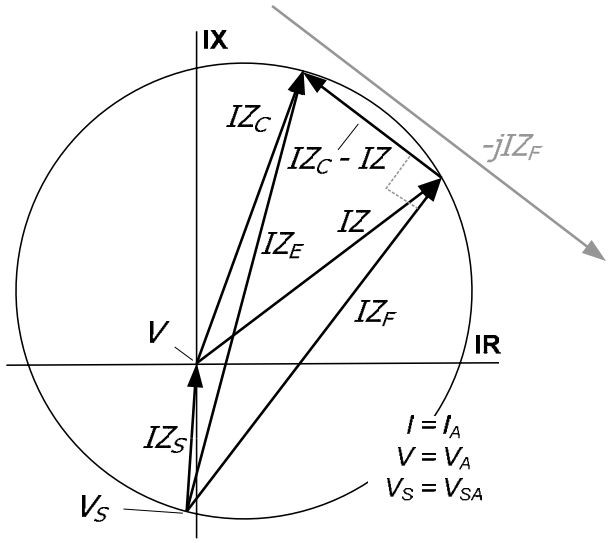

Fig. 3. Cross-polarized Mho Characteristic

The faulted phase source voltage, V_S, is evaluated based on healthy phase quantities. This is generally done by measuring the phase-to-phase voltage that is opposite the faulted phase, i.e. V_{BC} or V_{CB} is used for a fault on phase A (cross-polarized), or by computing and using the positive sequence voltage (positive sequence polarized). In this case for the comparator of Figure 1(a) we use the following values for the phase-A unit:

$$S_1 = V_{BC} \quad (6)$$

$$S_2 = I_A Z_C - V_A \quad (7)$$

Figure 4(a) shows how V_{BC} is related to V_{SA}. For balanced system voltage and no load we have:

$$V_{BC} = jV_{SA}\sqrt{3}$$

It is not the magnitude, but the angle of the polarizing quantity that is significant. Figure 4 also shows how V_{BC} is influenced by the source impedance and load. At no load the healthy voltages are approximately the same as the source voltages. However as load flows forward or reverse through the relay there will be a voltage drop across the source

impedance causing the polarizing quantity, V_{BC}, to shift its reference angle lagging or leading its no load position. The effect of load on the dynamics of a cross-polarized mho is shown in Figure 5. It is this dynamic characteristic that correctly adapts to the effect that forward and reverse load have on fault resistance providing correct operation around the reach boundary [2].

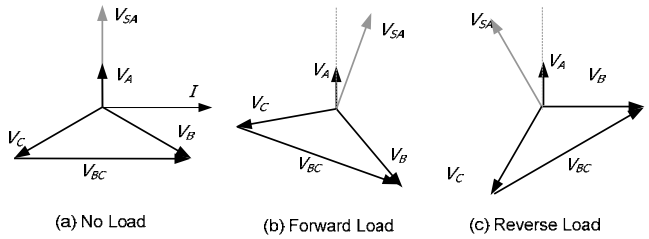

Fig. 4. Polarizing Quantity S1 (V_{BC}) Phase Shift Due to Load Direction

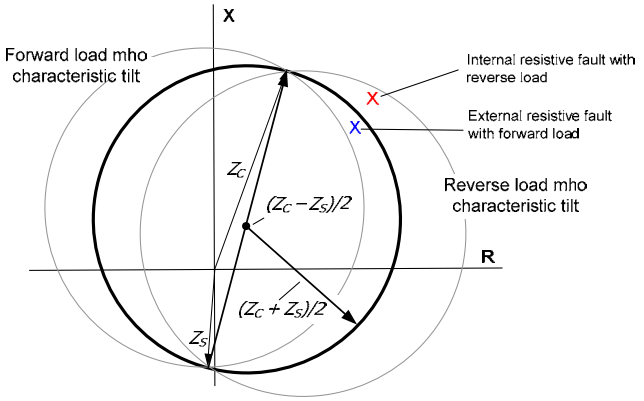

Fig. 5. Cross-polarized Mho Characteristic Dynamics

C. *Phase Comparator Based on Torque*

To this point we have only discussed the phase comparator that just compares the phase angle relationship of two phasors. The fault may be determined to be either within the operating characteristic or external to it. There is no information that indicates an internal fault is located "close-in" or near the operating boundary. This is achieved by torque measurement.

To introduce the subject of torque we will discuss the basic electromechanical phase comparator, which is also known as a cylinder unit. Its operation is described with Figure 6. This unit has two voltage inputs, S_1 and S_2. Each input is wound evenly on the two diametrically opposite poles of the stator of what is basically a 4-pole poly-phase induction motor.

Voltages applied at S_1 and S_2 generate fluxes Φ_1 and Φ_2 that induces currents in the armature (cylinder) that produce an operating or restraining torque depending on their phase relationship. Operating or restraining torque requires the presence of both S_1 and S_2 inputs that are measurable and not in phase or 180° out of phase.

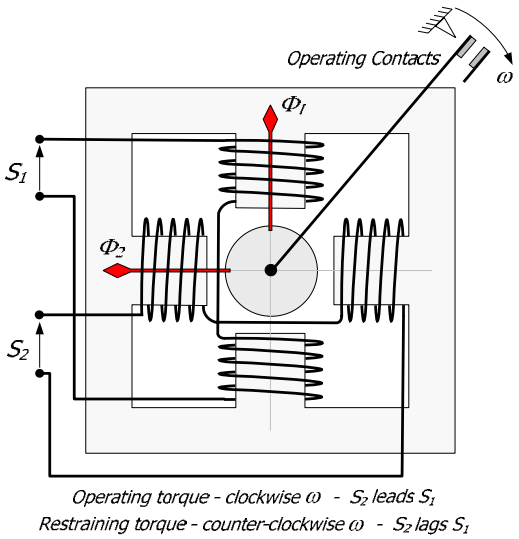

Fig. 6. Electromechanical Phase Comparator

To achieve operating or restraining torque, Φ_1 must lead or lag Φ_2 by some measurable quantity. This will set up a rotating magnetic field in one direction or another. For example, if Φ_2 lags Φ_1 this will setup a rotating magnetic field in the counter-clockwise direction. The rotation of the field acts upon the cylinder to rotate in the same direction. Likewise, if Φ_2 leads Φ_1 this will produce rotation in the clockwise or operating direction. The basic result is that torque to produce rotation in the operating or restraining direction is being produced and that its magnitude and direction, rather than the angular relation may be directly computed from the input quantities, S_1 and S_2. For the comparators of Figure 1(a) where S_2 leads S_1 for operation, the basic torque equation is:

$$T_q = \mathrm{Re}(S_1)\cdot\mathrm{Im}(S_2) - \mathrm{Re}(S_2)\cdot\mathrm{Im}(S_1)$$
$$= |S_1|\cdot|S_2|\sin(\varphi) \qquad (8)$$

Where the Re and Im indicate the real and imaginary components and

$$\varphi = \arg\left(\frac{S_2}{S_1}\right)$$

The significance of the torque equation is that it shows varying torque levels for different values of S_1, S_2 and φ. Consider the following phase comparator input quantities:

$$S_1 = -jV_{SA} \qquad (9)$$
$$S_2 = I_A Z_C - V_A \qquad (10)$$

And that

$$V_A = \frac{Z}{Z + Z_S} V_{SA} \quad (11)$$

$$I_A = \frac{V_{SA}}{Z + Z_S} \quad (12)$$

Then we have input values in terms of source voltage V_{SA} and source, compensator and fault impedances.

$$S_1 = -jV_{SA} \quad (13)$$

$$S_2 = \frac{Z_C - Z}{Z_S + Z} V_{SA} \quad (14)$$

We can now easily develop an expression for torque using (8), (13) and (14).

$$Tq = |V_{SA}|^2 \left| \frac{1 - Z/Z_C}{SIR + Z/Z_C} \right| \sin \varphi_P \quad (15)$$

where

$$\varphi_C = \arg(Z_C - Z)$$
$$\varphi = \arg(Z_S + Z)$$
$$\varphi_P = \varphi_C - \varphi + 90°$$
$$SIR = Z_S / Z_C$$
$$T_q \text{ is positive for } 0° < \varphi_P < 180°$$

This equation illustrates the effects of source, compensator and fault impedances on the amount of the torque produced. Figure 7 shows the plot of the normalized torque, T_q^{norm}, which is the computation of (15) with V_{SA} and sin φ_P set equal to one. It can be seen that that the torque is negative beyond the reach boundary, zero at the boundary, and positive within the protected zone. The smaller the fault impedance is, the greater the torque will be. For a specific fault location, the torque is inversely proportional to the SIR.

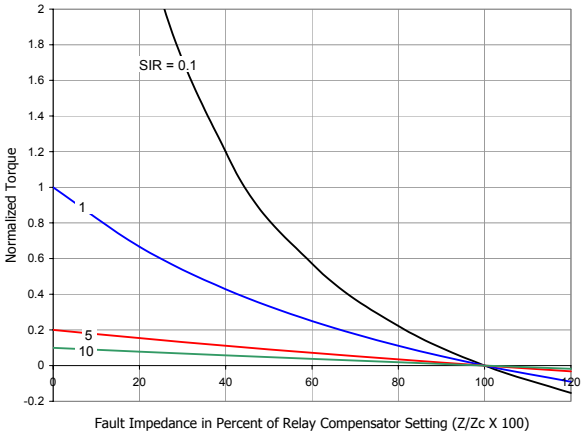

Fig. 7. Phase Comparator Torque Characteristics Based on SIR

IV. Application Issues

A. Dc Offset

Dc offset is a term generally associated with asymmetrical fault current for transmission line faults although it is present in voltage but to a lesser extent. The asymmetrical current has a fundamental frequency component and an exponentially decaying component, which is referred to as dc offset, whose time constant is dependent on the source and line inductive reactance and resistance and fault resistance. The initial offset magnitude is dependent on the source voltage and the current fault inception angle. The dc offset component in current is reflected in the voltage over the impedance in the system. If these quantities are accurately transformed to the secondary side of the instrument transformers and the impedance measurement is based on an accurate impedance model there will be correct correlation between the dc component in current and the dc component in voltage. If the filtering of current and voltage are done in similar ways, the dc component does not present a problem.

B. CCVT Subsidence Transient

Issues due to CCVT design and application were first observed in the latter 1960's with the first applications of solid-state line distance relays that provided high-speed sub-cycle operation relatively independent of the application's SIR. After extensive investigation into the causes of the incorrect overreach operations the problem was found to be due to the CCVT transient response to system faults. Extensive testing and analysis was done to define the different CCVT design parameters effects on the CCVT's transient response and the results were reported in reference [6]. Reference [7] discusses the validation of an equivalent circuit and provides frequency response characteristics of the CCVT with varying parameters. Reference [8] provides further study of the subject as it applies to microprocessor relays designed with DFT algorithms. Reference [9] addresses DFT distance relay application with bushing potential devices. A brief review of the issue as derived from these sources is provided.

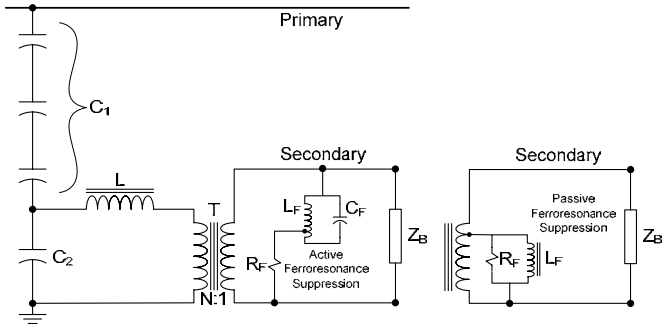

Fig. 8. CCVT Equivalent Circuit

The CCVT equivalent circuit is shown in Fig. 8 with the major components that affect the CCVT subsidence transient. These include the stacked and tapped capacitance C1 and C2, saturating reactor L, intermediate voltage transformer T, ferroresonance suppression circuit FSC and burden. The

CCVT is designed to pass the fundamental operating frequency, 50 or 60 Hz, with minimum error in magnitude and phase angle. It has a typical frequency response [7][8] as shown on Fig. 9 designed with either an active or passive FSC.

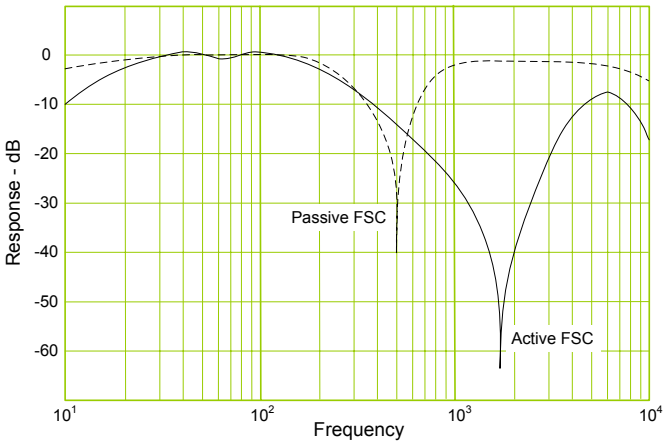

Fig. 9. CCVT Frequency-response Characteristic with Active or Passive Ferroresonance Suppression Circuit (FSC)

When a fault occurs on the protected line the voltage collapses on the primary of the CCVT and there is a transient voltage of generally one or two cycles introduced on the secondary of the CCVT due to the active inductive and capacitive CCVT circuit components. This transient does not appear in the primary system and therefore directly affects the DFT calculation of the protection's voltage fundamental frequency component, which makes the secondary voltage momentarily appear as a lower value than it actually is. This is particularly true for the CCVT with an active FSC due to its wide band frequency response characteristics. The CCVT designed with a passive FSC, which has a smaller frequency response band width, greatly reduces the overreaching effect of [DFT] distance relaying [8]. This demonstrates that narrowing the band width around the fundamental frequency will significantly reduce the overreaching effect, if not eliminate it.

Other CCVT parameters that affect the subsidence transient are shown in Table 1.

TABLE 1. CCVT PARAMETER EFFECT ON SUBSIDENCE TRANSIENT

Parameter	**Small Transient**	**Large Transient**
Stacked and tapped capacitance C_1 & C_2	Large	Small
Intermediate transformer T turns ratio N	Large	Small
Ferroresonance suppression circuit	Passive	Active
Burden Z_B	Resistive	Inductive

The system parameter that has the greatest effect on the CCVT subsidence transient is the Source to Line Impedance Ratio, SIR. From the protective relay's perspective, however, SIR is the ratio of the source impedance to the distance measuring zone's reach setting. A high SIR is indicative of a low fault voltage at the relay and thus where the change from normal pre-fault to fault voltage and likewise the subsidence transient are large. High SIR is also indicative of a short zone-1 reach setting where sensitivity to the CCVT transient error is greater.

V. NUMERICAL PHASE COMPARATORS

In the following discussion we will review two microprocessor phase comparator implementations and discuss advantages and disadvantages of each. These implementations are a phase comparator method that evaluates the phase relationship only using a Discrete Fourier Transform (DFT) method commonly used with microprocessor relaying. The second method is a time-based numerical comparator algorithm measuring accumulated torque energy.

A. Discrete Fourier Transform (DFT) Method

First, a basic overview of the principle of the Discrete Fourier Transform is provided. The sequence of N complex numbers $x_0, \ldots, x_{N-1}$ is transformed into the sequence of N complex numbers $X_0, \ldots, X_{N-1}$ by the DFT according to the formula:

$$X_k = \sum_{n=0}^{N-1} x_n e^{-\frac{j2\pi}{N} k n} \qquad k = 0,\ldots,N-1 \tag{16}$$

where $k = 0,1,\ldots,N-1$ denotes the different harmonics ($k = 1$ is the fundamental frequency signal with a cycle time equal to N samples), e is the base of the natural logarithm, j is the imaginary unit ($j^2 = -1$), and π is pi. e^{jx} can also be written in complex form as $cos(x) + jsin(x)$.

This gives that X_k can be interpreted as consisting of two orthogonal components which, using $cos(-x) = cos(x)$, can be written in complex form as

$$X_k = \sum_{n=0}^{N-1} x_n \left[\cos\left(\frac{2\pi}{N} k n\right) + j \sin\left(-\frac{2\pi}{N} k n\right) \right] \tag{17}$$

For use in relay protections the DFT value is normally calculated as Cartesian components, using the latest N samples according to formulas:

$$\mathrm{Re}(X) = \frac{2}{N} \times \sum_{i=0}^{N-1} x(i) \times \cos\left(i \times h \times \frac{2\pi}{N}\right) \tag{18}$$

$$\mathrm{Im}(X) = -\frac{2}{N} \times \sum_{i=0}^{N-1} x(i) \times \sin\left(i \times h \times \frac{2\pi}{N}\right) \tag{19}$$

It can also be converted into Polar format using the formulas:

$$Mag(X) = \sqrt{\mathrm{Re}(X)^2 + \mathrm{Im}(X)^2} \tag{20}$$

$$Ang(X) = \arctan\left(\frac{\mathrm{Im}(X)}{\mathrm{Re}(X)}\right) \tag{21}$$

Re = Real part , Im = Imaginary part, Mag =Magnitude and Ang = Angle of complex DFT phasor. h = harmonic to be calculated; 1 = Fundamental frequency, 2 = second harmonic, 3 = third harmonic etc. x(i) = i^{th} sample value in a buffer containing the N samples.

The DFT values can then be used in a phase comparator according to Figure 1 and equation (8).

Because of the inherent filtering of the DFT, no additional filtering is normally introduced for the evaluation. In some cases a low value trip counter is used, requiring a set number of evaluations to indicate trip before an output is given.

The polarizing input S1 normally uses cross-polarization or positive sequence voltage polarization. The operating input S_2 is the compensated voltage. For the phase A to ground measuring element it can be written as indicated in equation 1:

$$S_2 = I_A Z_C - V_A \qquad (22)$$

When creating S_2, DFT values are used for I_A and V_A. The DFT filtering responds not only to the fundamental frequency signal but also to transient components that are not filtered. In this case the transient component, especially from a CCVT, can cause overreach for reasons discussed in Section IV. The solution to limit the influence of the subsidence transient is to introduce a damping effect after the DFT filter. This is achieved by running the signal through a low-pass filter with a carefully selected bandwidth.

An example of such a case with low fault voltage due to high SIR and a high CCVT transient is shown in Figure 10. The pre-fault voltage is 63 V and the fault inception is at zero cycles.

Due to the transient component, there will be a fundamental damped oscillation in both magnitude and angle in the output from the DFT filter as shown in Figure 11. The angle is given in radians (1 radian is approx 57 degrees) to fit in same window as voltage. The steady state value for magnitude is about 2.3 V at an angle of -0.55 radians (≈ -90 degrees). The combined oscillation of voltage magnitude and angle can result in an overreach of almost 50%.

By introducing a low-pass filter with a suitable bandwidth, after the DFT filter, the oscillation can be damped as shown in Fig. 12 for the amplitude and Fig. 13 for the angle in degrees.

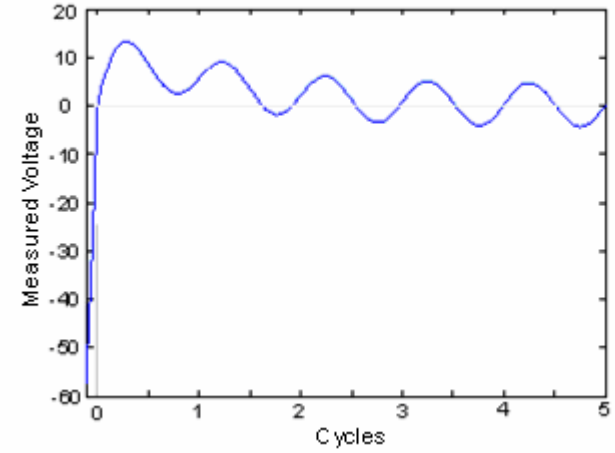

Fig. 10. Phase voltage for a high SIR fault with CCVT transient

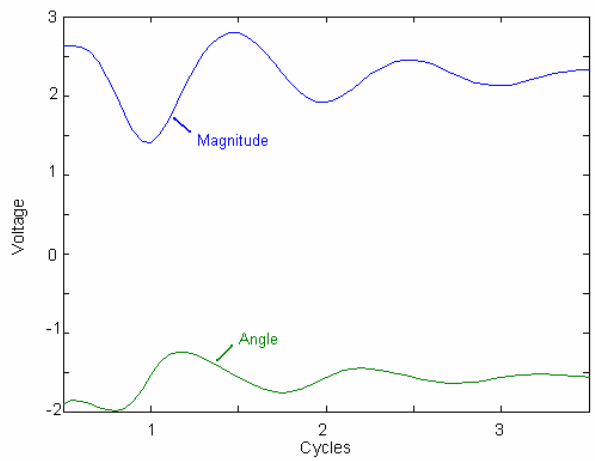

Fig. 11. Output from DFT filter

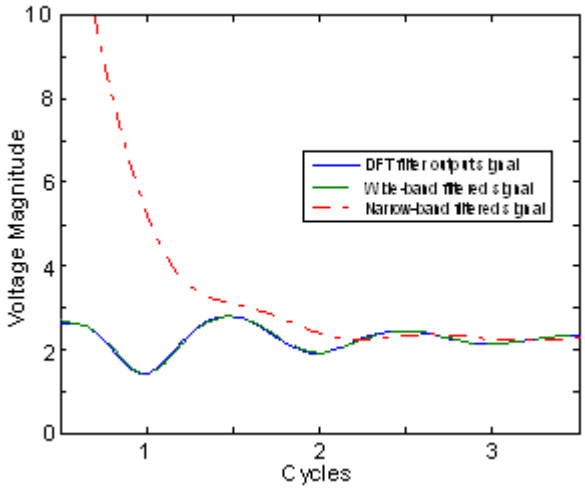

Fig 12. Voltage output from additional CCVT filter

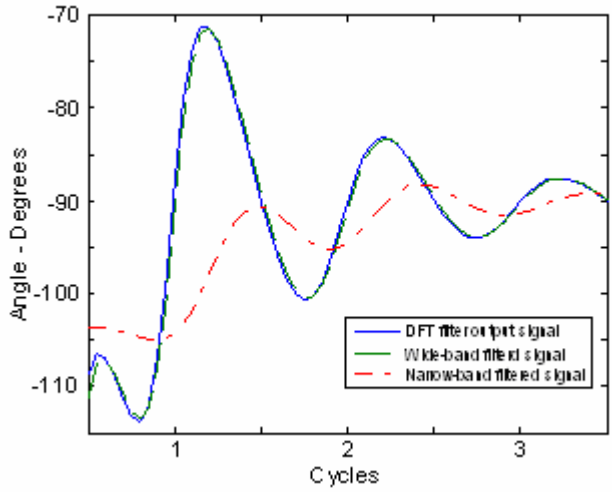

Fig. 13. Angle output from additional CCVT filter

The need is to minimize or eliminate the oscillations, particularly in magnitude, that affect the accuracy and cause undesired overreaching. The drawback of this is that filtering produces additional time delay. Instead of passing 2.3 V at 0.5 cycles (Fig. 12) without CCVT narrowband filter, it passes 2.3 V at about 2.2 cycles, resulting in an additional time delay of about 1.7 cycles.

For correct implementation of the DFT phase comparator two different bandwidths are used, one narrow for underreaching zones to prevent overreaching and one wider for overreaching zones where transient overreach is not critical but speed is important, particularly for pilot protection. Fig. 14 shows the DFT phase comparator operating characteristics using narrowband and wideband filtering.

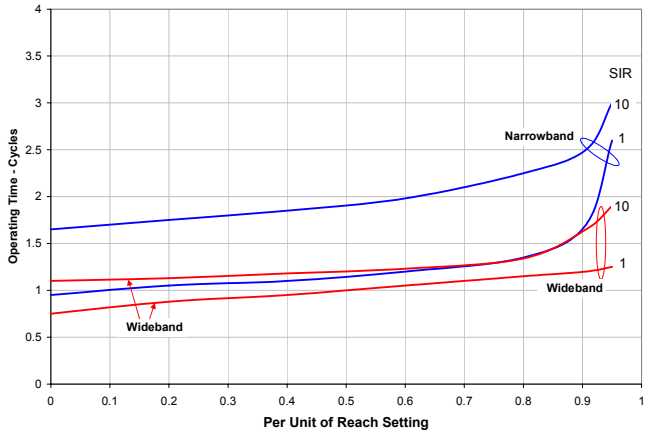

Fig. 14. DFT Phase Comparator Operating Time Using Narrowband and Wideband Filters. The narrowband is used for underreaching (zone-1) applications for security against transient overreach. The wideband is used on overreaching applications providing faster operations over a greater range of SIR applications.

B. *Time Based Torque Method*

Contrary to popular belief, electro-mechanical distance relays are quite fast. It is their torque-based operating characteristic that provides their immunity to fault transients such as those caused by CCVTs. If we plotted the inverse of the normalized value torque ($1/T_q^{norm}$) of Figure 7, the resulting curves as shown in Fig. 15 would be indicative of their operating speed characteristics for different fault locations, SIR levels and applied torque

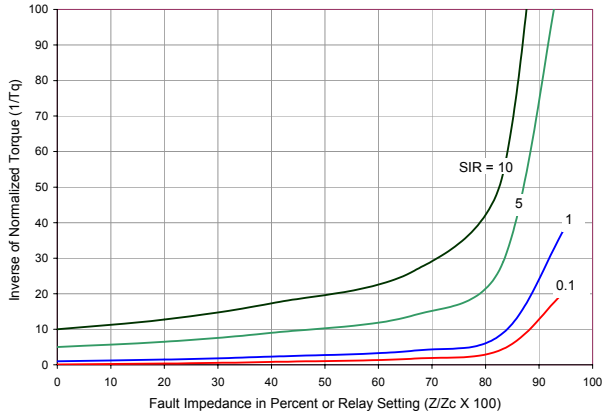

Fig. 15. Operation Characteristics of a Phase Comparator Based on Torque

Close-in faults (small Z/Z_C) result in relative fast operations while the operating time slows as the fault location approaches the relay reach, offering more security. To achieve the inherent advantages of this characteristic in a microprocessor relay, the development of numerical method in the time domain (TD) to accurately quantify torque was pursued.

1) *The Development of a Time Based Numerical Comparator*

The concept for a time based numerical comparator based on torque was introduced to the industry [2][3][4] in 1995 and was subsequently implemented in a transmission line protection product, which after extensive verification testing was released in 1997. The numerical comparator was again discussed at industry conferences [5] after a year of in-service application. The algorithm is adequately discussed in the aforementioned references, therefore, only a basic overview of the concept is provided here.

The concept is based on torque being applied to the rotating cylinder of Figures 5 and 16 and measuring its angular displacement (rotation), θ, in the trip direction as a function of time. Torque energy being applied to the cylinder's rotation as a function of input quantities S_1 and S_2 was defined in equation (8) and is now described in the continuous time domain in equation (23). The cylinder unit's angular displacement, θ, increases as long as torque is being applied in the trip direction, and if sustained the tripping contacts will eventually close. The applied torque must be sufficient to overcome several motion restraining factors. The angular displacement is defined in equation (24) where T_q is the result of (23), I is the cylinder unit's moment of inertia, and T_c, K_d, and K_c are opposing torque, damping and spring constants, respectively as described in Figure 16.

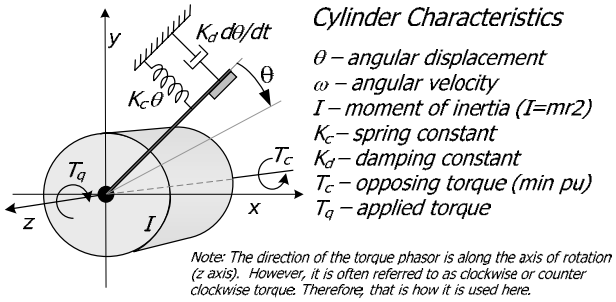

Fig. 16. Operation Characteristics of a Cylinder Unit

$$T_q(t) = S_1(t) \cdot \frac{d}{dt} S_2(t) - S_2(t) \cdot \frac{d}{dt} S_1(t) \qquad (23)$$

$$I \frac{d^2\theta}{dt} = (T_q - T_c) + K_d \frac{d\theta}{dt} + K_c \theta \qquad (24)$$

Equations (23) and (24) must be discretized in order to do sample to sample evaluation. This process is discussed in the aforementioned references, but a short discussion is provided to summarize the process. Equations (23) and (24) can be written in the discrete form as

$$T_q(k) = S_1(k) \cdot S_{2,\perp}(k) - S_2(k) \cdot S_{1,\perp}(k) \qquad (25)$$

$$\theta(k) = C_e\left[C_c\left(T_q(k) - Tc\right) + C_f\theta(k-1) - \theta(k-2)\right] \qquad (26)$$

Where S1,⊥(k) is the derivative of and is orthogonal to S1(k) at the fundamental frequency, and

$$C_e = \frac{I}{I + \Delta t K_d + \Delta t^2 K_c}$$

$$Cd = \frac{\Delta t K_d}{I} + 2$$

$$Cc = \frac{\Delta t^2}{I}$$

k = the sample number, k^{th} sample

Δt = time between samples

$T_q(k)$ is the instantaneous value of torque being applied to rotate the theoretical cylinder unit ant the k^{th} sample. The angular displacement $\theta(k)$ is a measure of accumulated (integrated) torque energy. The computation process is illustrated in Figure 17.

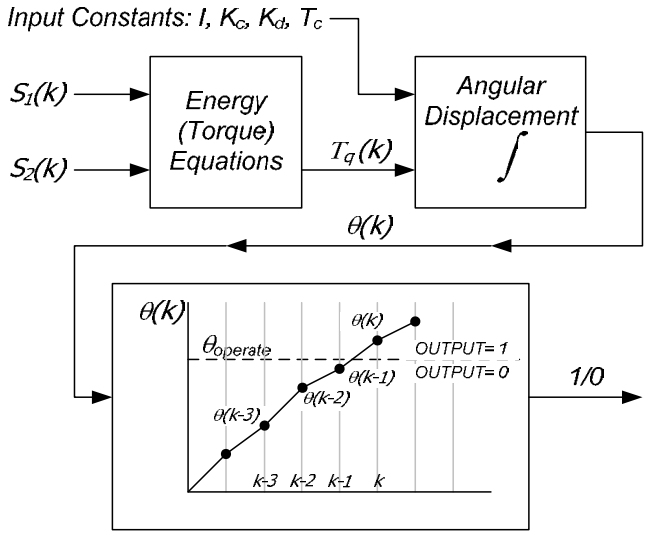

Fig. 17. Time Domain Numerical Comparator Block Diagram

The characteristics of numerical phase comparator units developed to address specific fault loops, phase-to-phase for example, are very similar to their electromechanical counterpart since the behavior of the cylinder unit is the basis of the numerical comparator. However, the exact representation of the cylinder unit was not the intent, but rather the development of useful and flexible expressions to be applied to protective relaying. One form of flexibility is the appropriate selection of constants to design the desired operating characteristics to provide operating speed and at the same time make the unit less susceptible to transients from the power system. For example decreasing the moment of inertia, I, is like decreasing the mass such that less energy is required to turn the cylinder and increasing the spring constant, Kc, will slow the rate of change of angular displacement, θ, as it increases.

2) 10 Years of Service

A product using time based numerical phase comparators has been applied over the past 10 years in thousands of transmission line protection applications. The operating characteristics showing the operating time as a function of fault location and SIR is shown in Figure 18[10].

In regard to the use of the unit for underreaching applications it has performed flawlessly for in-service applications on medium and long lines, SIR less than four [11], providing high-speed tripping for internal faults up to 95% of the reach setting and immunity to the application issues of external faults identified in Section III - all of this with zone-1 settings up to 90% of the line length. In-short, there have been no reported zone-1 non-operations for internal faults or operations for external faults, either forward or reverse.

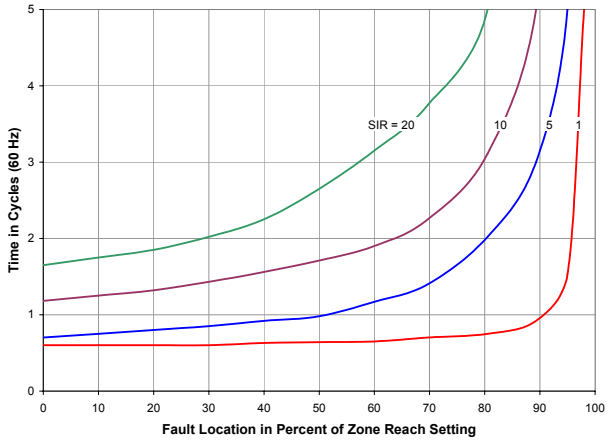

Fig. 18. Operating Characteristics of a Time-based Numerical Comparator Relay. SIR is the source impedance to the zone reach setting ratio. SIR values of 1, 5, 10 and 20 are shown.

Short lines are defined as having an SIR greater than four and pilot applications are recommend to assure high-speed tripping at all terminals[11]. However, reality shows that many utilities apply zone-1 down to the lowest levels permitted by the relay design. Therefore, attempts to rely on zone-1 with SIR levels greater than four are not uncommon. As the SIR application levels increase, particularly for levels greater than 10, the problem with the time-based numerical comparator becomes one of dependability to provide reasonable tripping times for all faults within the reach setting, particularly those faults in the last 20% to 30% of the reach setting.

For pilot application utilizing overreaching zones there are no issues even for short line applications. For medium and long line applications the maximum fault impedance will be 66.67% of the normally applied overreaching setting of 150%

of zone-1 reach. Modern microprocessor relays also provide separate zones for step-distance zone-2 and overreaching pilot measurement, thereby not restricting the pilot zone reach to the rules for applying zone-2. For very short line applications the setting criteria for the overreaching pilot zone is to set the reach such that the SIR for that setting is less than or equal to five. This assures high-speed pilot tripping.

There are also testing issues using conventional test-sets that occur due to the inverse characteristic and the tester's lack of familiarity with them. These usually take the form of underreaching or non-operations due to too short of a test interval (duration of applied fault) and a high *SIR* test. That is, for a given test SIR_T, the test quantities must be applied with sufficient time to allow operation. The test SIR_T does not always reflect, and is usually higher than, the actual application *SIR*. SIR_T can be estimated as

$$SIR_T = \frac{1 - V_T}{V_T} \qquad (27)$$

where V_T is the test voltage in per unit of the relay's rated input voltage.

C. Complementary Use of TD and DFT Algorithms

Parallel operation of the proven TD and DFT phase comparators are implemented to maintain the high-speed performance and overcome the testing and high SIR application issues of the TD phase comparator. The DFT phase comparator complements the TD comparator by limiting the maximum operating time from 2.0 to 4.0 cycles depending on SIR and fault location. Figures 19 and 20 show the effective TD/DFT operating characteristics for underreaching and overreaching applications.

Zone-1 (Fig. 19) provides reliable high-speed operation for moderate to low SIR values with the TD algorithm and very reasonable operating times with the DFT for higher SIR values. The operating time for pilot protection, which utilizes overreaching distance measurement (Fig. 20), is improved further for higher SIR values by the omitting narrowband filtering that is not required on the overreaching zones.

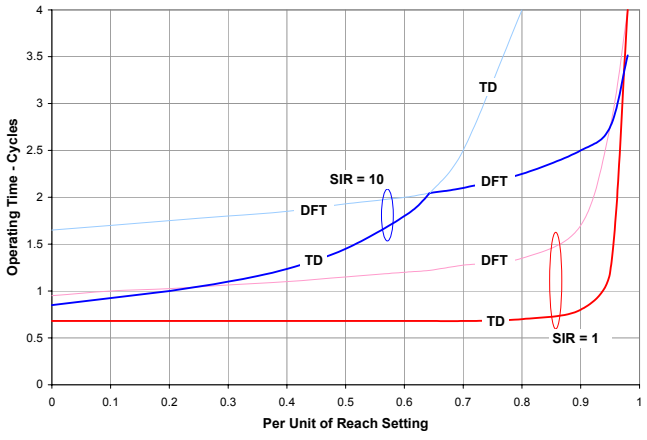

Fig. 19. Operating Characteristics of Combined TD and DFT Phase Comparators for Underreaching Applications (Zone-1)

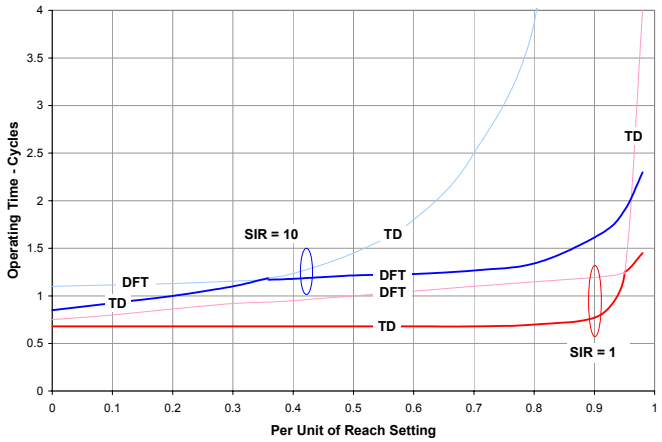

Fig. 20. Operating Characteristics of Combined TD and DFT Phase Comparators for Overreaching Applications (Zone-2, 3, Pilot)

VI. Conclusion

The mho-distance phase comparator principle was reviewed providing basic understanding of its dynamic operation. Also reviewed was the CCVT subsidence transient issue that compromizes security on zone-1 applications. Two distinctly different phase comparator numerical methods, TD and DFT, were discussed addressing basic design, operating performance and their respective issues related to speed, dependability and security. Finally, it was shown that with the combined use of the two application-proven phase comparators operating in parallel, overcame each method's shortcomings providing reliable high-speed performance.

References

[1] W. A. Elmore, *Protective Relaying: Theory and Application,* Marcel Decker, Inc., 1994.

[2] W. A. Elmore, F. Calero, L. Yang, "Evolution of Distance Relaying Principles," *49th Annual Georgia Tech Protective Relaying Conference*, May 3-5, 1995, Atlanta, Georgia.

[3] F. Calero, "Development of a Numerical Comparator for Protective Relaying: Part I," *IEEE Transactions on Power Delivery*, Vol. 11, No. 3, July 1996, pp. 1266 – 1273.

[4] D. Hart, D. Novosel, F. Calero, E. Udren, L. Yang, "Development of a Numerical Comparator for Protective Relaying: Part II," *IEEE Transactions on Power Delivery*, Vol. 11, No. 3, July 1996, pp. 1274 – 1280.

[5] L. Wang, E. Price, "High-speed Microprocessor Distance Relaying for Transmission Lines, " *25th Annual Western Protective Relay Conference*, Oct. 13 – 15, 1998, Spokane, Washington.

[6] A. Sweetana, "Transient Response Characteristics of Capacitive Potential Devices," IEEE Transactions on Power Apparatus and Systems, Vol. 90 No. 5, , September, 1971, pp 1989 – 2001.

[7] M. Kezunovic, C. Fromen, S. Nilsson, "Digital Models of Coupling Capacitor Voltage Transformers for Protective Relay Transient Studies," IEEE Transactions on Power Delivery, Vol. 7, No. 4, Oct. 1992, pp 1927 – 1935.

[8] D. Hou. J. Roberts, "Capacitive Voltage Transformers: Transient Overreach Concerns and Solutions for Distance Relaying," 22nd Annual Protective Relay Conference, Oct. 24 -26, 1995, Spokane, Washington.

[9] D. Angell, D. Hou., "Input Source Error Concerns for Protectivr Relays," 33rd Annual Protective Relay Conference, Oct. 2006, Spokane, Washington.

[10] *REL512 Line Distance Protection Terminal, Instruction Book*, ABB Inc., Allentown, PA, 2001

[11] *IEEE Guide for protective Relay Applications to Transmission Lines*, IEEE Std. C37-113, 1999

VII. BIOGRAPHIES

Elmo Price received his BSEE degree in 1970 from Lamar University in Beaumont, Texas and his MSEE degree in Power Systems Engineering in 1978 from the University of Pittsburgh. He began his career with Westinghouse in 1970 and worked in many engineering positions that included assignments at the Small Power Transformer Division in South Boston, VA, the Gas Turbine Systems Division in Philadelphia, and T&D Systems Engineering in Pittsburgh. He also worked as a District Engineer located in New Orleans and supporting the South-central U.S. With the consolidation of Westinghouse into ABB in 1988 Elmo assumed regional responsibility for product application for the Protective Relay Division. From 1992 to 2002 he has worked at both the Coral Springs and Allentown Divisions in various technical management positions responsible for product management, application support and relay schools. Elmo is currently Regional Technical Manager for ABB in Dawsonville, Georgia supporting product sales and application in the southeastern U.S. Elmo is a registered professional engineer and a senior member of the IEEE. He is also a member of the PSRC and the Line Protection Subcommittee, serving as a contributing member to many working groups. Elmo's email address is elmo.price@us.abb.com

Torbjorn Einarsson received his MScEE degree in Electrical Engineering in 1972 from the Chalmers Technical University, Gothenburg, Sweden. He joined ASEA (becoming ABB after the merge with BBC), Sweden in 1973 as a Test Engineer for High Power testing. In 1977 he moved to Protective Relay Division as Development Engineer and is currently is a Development Project Manager for protective relays at ABB AB, Vasteras, Sweden. He has been appointed as Specialist in Line Protection. His areas of interest are communication for line protection systems and development and testing of line protection relays with special focus on line differential protection. Torbjorn's email address is torbjorn.einarsson@se.abb.com